Accepted Manuscript

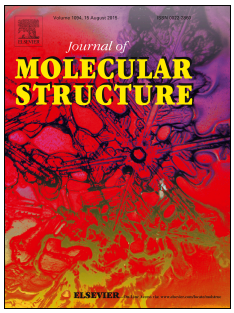

Synthesis for novel VO(II)- triazole complexes; spectral, analytical characterization and catalytic usage for biodiesel synthesis from waste oil

Nashwa El-Metwaly, Thoraya A. Farghaly, Ismail Althagafi, Marwa G. Elghalban

PII: S0022-2860(19)30407-7

DOI: https://doi.org/10.1016/j.molstruc.2019.04.018

Reference: MOLSTR 26390

To appear in: *Journal of Molecular Structure*

Received Date: 10 February 2019

Revised Date: 2 April 2019

Accepted Date: 3 April 2019

Please cite this article as: N. El-Metwaly, T.A. Farghaly, I. Althagafi, M.G. Elghalban, Synthesis for novel VO(II)- triazole complexes; spectral, analytical characterization and catalytic usage for biodiesel synthesis from waste oil, *Journal of Molecular Structure* (2019), doi: https://doi.org/10.1016/j.molstruc.2019.04.018.

Graphical Abstract

Synthesis for novel VO(II)- triazole complexes; spectral, analytical characterization and catalytic usage for biodiesel synthesis from waste oil

Nashwa El-Metwaly* | **Thoraya A. Farghaly** | **Ismail Althagafi** | **Marwa G. Elghalban**

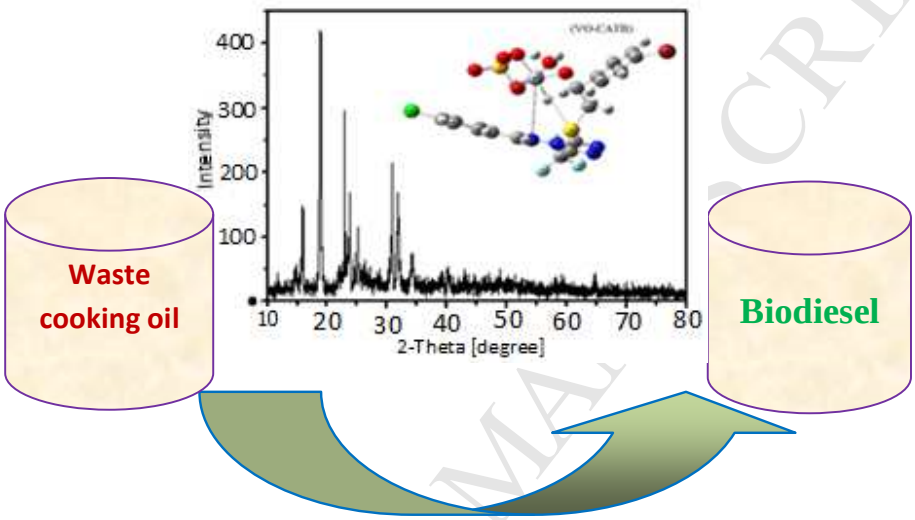

Synthesis for novel VO(II)- triazole complexes; spectral, analytical characterization and catalytic usage for biodiesel synthesis from waste oil

Nashwa El-Metwaly[a,b*] | Thoraya A. Farghaly[a,c] | Ismail Althagafi[a] | Marwa G. Elghalban[a,b]

[a]*Chemistry Department, College of Applied Sciences, Umm Al-Qura University, Makkah, Saudi Arabia*
[b]*Chemistry Department Faculty of Science, Mansoura University, Mansoura, Egypt*
[c] *Chemistry Department, Faculty of Science, Cairo University, Cairo, Egypt*

ABSTRACT

Novel mono-nuclear VO(II)-traizoles complexes have been synthesized and fully characterized by all possible tools(analytical, spectral and conformational). The neutral tri-dentate mode, was the suggested bonding feature based on comparative IR spectra. The octahedral geometry, was suggested for all complexes except for $[VO(CATP)(H_2O)]$ $(SO_4)(H_2O)_2$ complex. ESR spectral data clarify, the ionic feature of in plane σ- bonding as well as in plane π - bonding. XRD patterns display the amorphous feature, as the main characteristic for most tested compounds. Two crystalline complexes, showed crystallite-sizes located excellently in nanometer range. SEM images displayed rocky-shape surfaces for all tested compounds, except for the two crystallite complexes. TGA curves displayed discriminated thermal stability, among investigated complexes, which most of them appeared with high thermal stability. Conformational indexes calculated predict the superiority features of $[VOSO_4(CATB)]H_2O$ complex. This study was strengthen by docking process, which orients to the negligible inhibition role of most VO(II)-complexes against DNA (2hio). Another application pathway was interested to synthesize biodiesel from waste oils. A chosen complex (VO(II)-CATB) was utilized in heterogeneous-catalytic process. Moreover, its V_2O_5 oxide has been prepared from deliberate calcinations process. The complex and its oxide have been used separately to prepare economic compound (biodiesel) from waste oil. The two catalysts succeeded in isolating biodiesel, in particular the complex which produced a perfect product in record time. Some physical characteristics were estimated for synthesized biodiesel, which highly compatible with that reported in literature for other undesirable biodiesel-synthesis processes.

Keywords: VO(II)-Traizole complexes, Biodiesel synthesis, Molecular Docking, DFT/B3LYP

[*]*Corresponding author:* Prof. Nashwa M. El-Metwaly

E- mail address: n_elmetwaly00@yahoo.com , *Telephone No.: +966538553123*

1. INTRODUCTION

One of the challenges facing industry and many sectors in the world is the lack of energy sources. Scientists around the world are searching for cheap and easy-to-access sources of energy. The curtailment fossil fuel reserves and more rigorous environmental assizes have produced a global concern in renewable energy sources. The alternative fuel, biodiesel, is generated from the trans-esterification by alcohols of animal fats or vegetable oils [1]. The properties of biodiesel are similar to those of petroleum-diesel and can be used in traditional diesel engines without amendment. Biodiesel is less toxic, renewable and has minimal environmental effect compared to diesel extracted from petroleum [2]. The limitation of the production of biodiesel is attributed to high costs of raw material, vegetable oils [3]. Also, using the edible oils in the production of biodiesel will be affected on the existing food market. So, the researches over the worldwide have focused on biodiesel production from WCO(Waste Cooking Oil) as a third generation source which have a positive effect on the efficiency of such fuel[4,5]. The tras-estrification with homogenous catalysts such as KOH and NaOH has some advantages as low price and easy availability, but the catalyst cannot be reused. Furthermore, it gives soaps when reacts with oil and acids, which reduces the percent yield of esters, make the detachment difficult and also consume the catalyst and cannot be isolated from the reaction mixture. So, using heterogeneous catalysts especially metal oxides is the suitable solution to these problems[6,7].On the other hand, the discovery of vanadate-dependent enzymes and their significance in diverse biological catalytic operations [8,9] has spurred research on the catalytic manifestations of vanadium (VOLx) complexes. Several pattern vanadium complexes display catalytic activity towards different organic conversions, also, VO(II)-nitrogen coordination plays a good role in catalysis of nitrophenol to aminophenol[10,11].Triazoles and their Schiff's bases displayed outstanding pharmacological activities as anticonvulsant, antimicrobial, antitumor, analgesic, and antidepressant[12]. From the previous work reported, we intended to synthesize new VO(II)-traizole complexes. These complexes will be fully characterized using all possible spectral, analytical and theoretical techniques. Two selected complexes will be tested towards biodiesel synthesis from waste oil. Moreover, their oxides yielded from calcinations will be used in this catalytic application after full description. This heterogeneous catalytic process, will be compared versus referenced undesirable method, which mainly used a dangerous catalyst (CaO). This study, aims to throw a shadow on a new distinguish catalyst used to synthesize economic product from wastes by a safe process.

2. Methodology

2.1. The reagents

All chemicals, reagents and solvents were purchased from Fluka, Merck and Sigma-Aldrich. Also, used as it is without previous treatments. $VOSO_4.XH_2O$, trifluoroacetic acid, thiocarbohydrazide, 4-chlorobenzaldehyde, 2-bromo-4′-aminoacetophenone, 2-bromo-4′-methylacetophenone, 2-bromoacetophenone, 2-bromo-4′-chloroacetophenone and 2-bromo-4′-bromoacetophenone, were the compounds utilized in the synthesis for new compounds.

2.2. Preparations

2.2.1. Synthesis of triazole derivatives

A scientific preparation method for 4-amino-5-trifluoromethyl-4*H*-[1,2,4]triazole-3-thiol (**3**) was reported in previous work[13].As; equi-moles from aqueous trifluoroacetic acid (**1**) (11.4g, 0.1 mol) and thiocarbohydrazide (**2**) (10.6g, 0.1 mol) were mixed and refluxed along 5h, then cooled. The white crystals obtained were isolated through filtration followed by washing with cold water and re-crystallized from water to produced pure triazole compound **3**. Conversion of triazole derivative **3** to 4-((4-chlorobenzylidene)amino)-triazole-3-thiol derivative **4** carried out *via* the condensation of aminotriazole thiol **3** (4.6g, 0.025 mol) with 4-chlorobenzaldehyde (3.5g, 0.025 mol) in glacial acetic acid (20 mL) under conventional heating for 5 h followed by filtration for the formed precipitate and crystallization from ethanol. New traizole compounds (6a-e, Scheme 1) were isolated from the reaction of equi-moles (3.06g, 0.01 mol) from compound **4** and α-haloketone derivatives (**5a-e)** (2.12g **(5a)** or 2.13g **(5b)** or 1.98g **(5c)** or 2.31g **(5d)** or 2.76g **(5e),** 0.01 mol**) .** Each reaction mixture was refluxed in dioxane (30 ml) in presence of 0.35 mL triethylamine a long 8-10 h (tested regularly by TLC (1:1, ethylacetate : *n*-hexane). The solid precipitates were filtrated off and re-crystallized from proper solvent. The best structural form for five derivatives was displayed (Fig. 1).

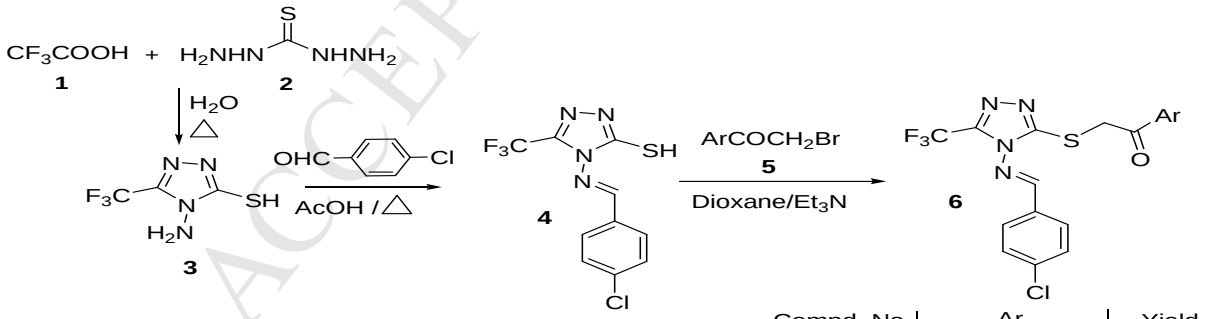

Compd. No.	Ar	Yield
6a	4-$NH_2C_6H_4$	78%
6b	4-$CH_3C_6H_4$	80%
6c	C_6H_5	75%
6d	4-ClC_6H_4	72%
6e	4-BrC_6H_4	70%

Scheme 1. Synthesis of ligands **6a-e**

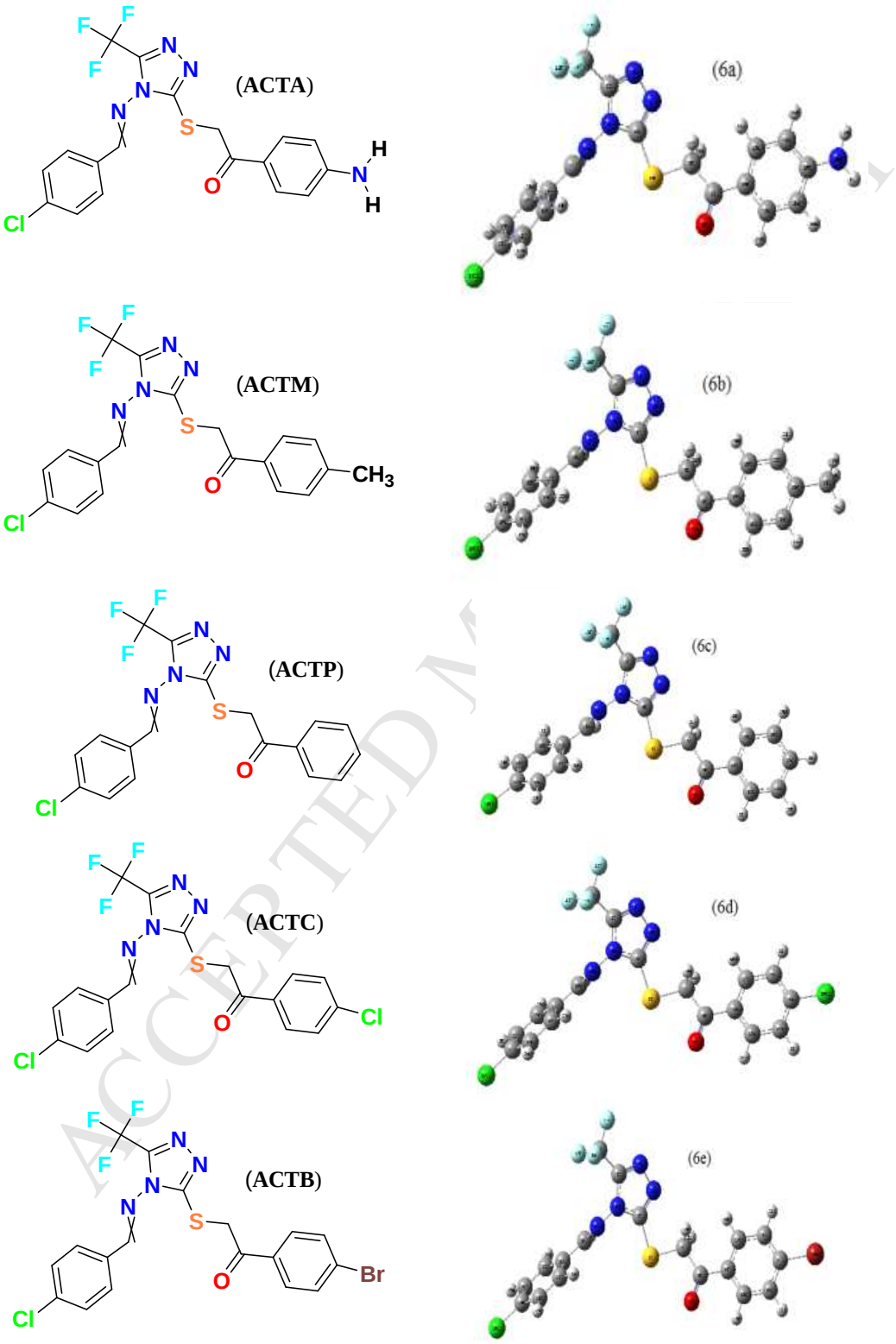

Fig. 1. Optimized structures of traizole derivatives (**6a-e**; CATA-CATB)

2.2.2. Preparation of VO(II)-traizole complexes

Novel colored VO(II)- traizole complexes were synthesized by mixing equi-molar weights. Dissolving 2mmol from $VOSO_4.xH_2O$ (neglecting hydrated water, 0.326g), then added to ethanolic solutions of traizole derivatives (6a-e) as follow, 0.880, 0.878, 0.850, 0.919 and 1.01 g, sequentially. All mixed solutions were refluxed for 4-7h. Dissolved 0.5 g sodium acetate (in bi-distilled water), was added to adjust pH of each solution for precipitation. The colored precipitates were isolated after filtration and washed by ethanol, diethyl ether and finally dried in vacuum desiccators.

2.3. Analysis techniques

The percentages of elements (carbon, hydrogen and nitrogen) were extracted by implementing Perkin-Elmer 2400 CHN Elemental Analyzer. The metal and sulfur contents were evaluated using standard analytical methods [14]. The conductance measurements (in DMSO) were recorded by JENWAY model 4070 Conductance Bridge. KBr-IR and NMR spectra were scanned over JASCO FT-IR-4100 spectrophotometer (400-4000 cm^{-1}) and Burker (500MHz), respectively. The electronic spectra and magnetic susceptibility were obtained through UV_2 Unicam UV/Vis spectrophotometer (in DMSO solvent) and Johnson Matthey Magnetic Susceptibility Balance at 25 ^oC, respectively. Mass spectra for two selected complexes were conducted at70 ev by using AEIMS 30 mass spectrometer using 40°C/min, heating rate and the mass/ charge scanning range was 50-1000. EPR spectra were given at 25 ^oC by using Jeol JES-RE1X EPR spectrometer with DPPH standard (υ = 9.435 GHz). TGA/DTG curves were extracted by Shimadzu Thermogravimetric Analyzer (20-900^oC). The heating rate was 10 ^oC min^{-1} under nitrogen. XRD patterns were obtained ($10^\circ<2\theta<90^\circ$ rang) on X-ray diffractometer (GNR, APD2000PRO, Italy) with a graphite mono-chromator. The scanning rate is 0.03° min^{-1} by using Cu/Kα1 radiation. SEM images were displayed on Joel JSM-6390 equipment. Molecular modeling and docking were executed by Gaussian09 and Autodock tools 4.2, respectively. DNA degradation was achieved in molecular biology lab.

2.4. Computational studies

2.4.1. Kinetics

ΔH, ΔS and ΔG were the thermodynamic parameters intended for computation over DTG curves. The order (n) and energy of activation (E) were also calculated over chosen stages. Well identified bordered, was the significant characteristic for chosen stages, which varied completely upon investigated curves. Many researchers [15-23] had accomplished equations for calculating these

parameters and discussing the advantages for such calculations in raising the knowledge about the prepared compounds and orient for application. Coat-Redfern[17] and Horowitz-Metzger[22], among the researchers interested in this point of research and developed equations for such purpose. These equations were implemented to calculate thermodynamic parameters over definite stages in DTG curves.

2.4.2. DFT/B3LYP method

The molecular optimization process, was performed by implementing Gaussian 09 program [24]. All triazole derivatives and their VO(II) complexes, were treated by using DFT/B3LYP method at suitable base set. Log and chk files were extracted and visualized upon Gauss-View program [25].All atoms were numbered according to scientific scheme. Essential parameters were extracted from output files, especially for E_{HOMO} and E_{LOMO} levels. Also, significant physical parameters were estimated by using known relations [26, 27], as follow;

1- $\chi = -0.5 (E_{LUMO} + E_{HOMO})$

2- $\mu = - \chi = 0.5 (E_{LUMO} + E_{HOMO})$

3- $\eta = 0.5 (E_{LUMO} - E_{HOMO})$

4- $S = -0.5 \eta$

5- $\omega = \mu^2 / 2 \eta$

6- $\sigma = 1/\eta$

2.4.3. QSAR study

Surface area, hydration energy, reactivity, Polarizability and Log p are the essential QSAR parameters calculated. HyperChem program (8.1) was used for optimizing the structural forms for ten tested compounds. Molecular mechanics force field (MM^+) followed by semi-empirical AM1 is considered the Pre-optimization process. A free optimization process was executed without restriction for any parameter till reaching the equilibrium state. Polake-Ribiere conjugated gradient algorithm was the system for minimizing energy content till reach the optimized structures [28].

2.4.4. Docking process

DOCK module of MOE technique (version 2014) [29,30] caused a great revolution in drug industry. Which is considered the pre-computational method in drug designing. Upon 2hio DNA receptor, the hydrogen atoms were added after removing water molecules around the duplex. MMFF94x force field, assigns the parameters and charges. Five VO(II) complexes were docked inside minor and major grooves, after generating alpha-site spheres using MOE site-finder module. The

docking scoring by MOE software in London dG scoring function and also upgraded by two unrelated refinement methods. The geometries of docking complexes were built in the best stereo and minimal energy, to be suitable for obtaining the best binding. The free binding energy and hydrogen bonds in between amino acid in the receptor, were used to clarify the grad of binding between the tested compounds and protein molecule. The hydrogen bonds were counted based on measuring the bond length, which is not exceed than 3.5 Å.

2.5. Biodiesel synthesis

The synthesis of biodiesel from cooking waste oils, is considered the main application interested in this study. The previous articles which interested in biodiesel synthesis, were mainly focus on using living lime (CaO) as a catalyst [31-33]. This catalyst is known by its high activity which needs restricted precautions during the experiment. Our process characterized by its safety and economic. First of all, the cooking waste oil obtained (WO) was filtered off to separate solid disposal before trans-esterification process.

2.5.1. Heterogeneous catalysis

A. Using prepared complexes

[$VOSO_4$(CATB)] complex was chosen as a potential catalyst in biodiesel synthesis. This choice was based on its expected reactivity, broad surface area and nano-crystalline nature as well as its thermal stability (till 147.8°C). In a round flask, 0.25g from the complex was mixed with 30 mL waste oil and (30 mL) methanol. The reaction mixture was stirred under reflux at 120°C for 2h. After refluxing a mixture, the complex was filtered off by centrifuge, dried and then weighed to assert on its catalytic role. After that, the reaction mixture was transferred to separating funnel, after 20 min, a perfect separation was observed for two phases. The biodiesel, the less dense phase (upper layer), was separated, washed with water then add NaCl to turn the solution clear, dried using Na_2SO_4 (anhydrous) then weighed

B. Using prepared oxides

A yellow powdered oxide, was obtained from previous complex, through calcinations process. This calcinations was carried out over a chosen complex in open air and then put in ignition oven (at; 650 ^oC) for complete calcinations till a constant weight. The oxide obtained was analyzed (elemental, XRD and SEM) to establish their chemical formulae. The reactivity, surface area and whole

morphology may be significantly different from similar purchased. The heterogeneous catalytic process (using complex) was repeated by using the prepared oxide (0.25g), for comparison. Also, such proposed heterogeneous catalytic process, was asserted by high degree of insolubility for the complex in the reaction medium, as well as the oxide used (V_2O_5). Moreover and after filtrating the catalyst, the weight used was completely unchanged before and after the process execution.

3. RESULTS AND DISCUSSION

3.1. General features

General features estimated from analytical study (Table 1), propose 1:1 molar ration among the ligand and vanadyl atom. The prepared complexes are stable, non hygroscopic, having high melting points (>300^{o}C). All synthesized complexes are insoluble in common organic solvents except DMSO and DMF were completely soluble. The molar conductivities (Λ_m) were measured for all complexes in DMSO solvent. The values computed were found at 5.41-51.75 $\Omega^{-1}cm^2mol^{-1}$ rang, which covering conducting and non-conducting features [34]. [VO(CATP)(H_2O)](SO_4)(H_2O)$_2$ and [VO (CATC)(H_2O)$_2$] (SO_4) complexes, were the conducting among the whole tested complexes. This may be discussed based on the contribution of ionizable sulphate group around the coordination sphere

3.2. Mechanism of triazole preparation

4-Aminotriazole thione **3** and its schiff base 4 were synthesized previously as described in literature reports [13]. The novel five ligands namely, 4-((4-chloro-benzylidene)-amino)-5-trifluoromethyl-3-(aryl)-2-oxoethyl)thio-4*H*-[1,2,4]triazole were prepared by refluxing a mixture of equimolar quantity of α-haloketone derivatives 5a-e and schiff base 4 in dioxane in the presence of base catalyst Et_3N. Studying all spectral data (Tables 2& 3) of the products, proved their structural forms. As for example, the ^{1}H-NMR spectra of all derivatives (Figs. 2 &1S) revealed in addition to the characteristic signals for the aromatic and aliphatic protons, the presence of singlet signal due to the methylene protons (CH_2) at δ 3.74-4.80 ppm. The mechanism for the formation of ligands was illustrated in Scheme 2. Moreover, IR spectrum of **6a** exhibited the characteristic absorption bands for stretching vibrations of NH_2 group at υ = 3434 and 3152 cm^{-1}. In addition, all derivatives revealed the absorption bands near 1680 cm^{-1} in their IR spectra, which attributed to the presence of carbonyl groups in CO-Ar moiety.

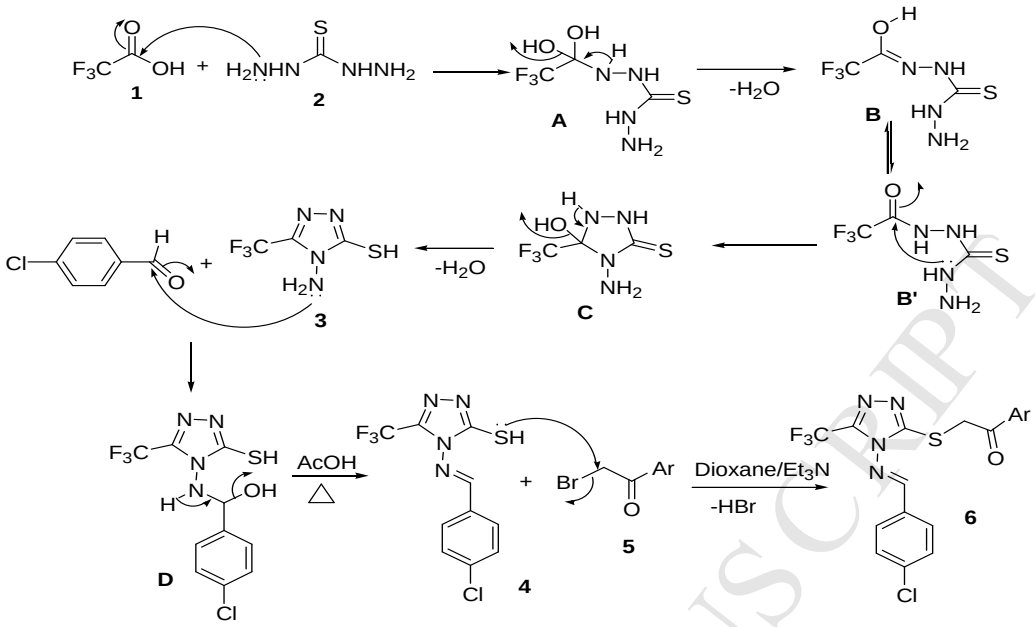

Scheme. 2. The mechanism of synthesis procedure for triazole derivatives (**6a-e**)

3.3. The mode of bonding in complexes

The mode of binding belonging to triazole derivatives (6a-e) toward VO(II) ions, was established based on relative shifts of function bands wavenumbers, after coordination. Table 3 summarize essential functional bands which point to bonding attitude. ν(C=O), ν(C=N) and ν(C-S) bands suffer a noticeable lower shift which refers to covalent coordination with VO(II) atom. This reflects the tridentate mode of bonding for triazole derivatives. $\nu_{as}(SO_4)$ and $\nu_s(SO_4)$ bands have been observed at; 1252-1289 and 1158-1191 cm^{-1} ranges in $[VOSO_4(CATA)]$, $[VOSO_4(CATM)]2H_2O$ and $[VOSO_4(CATB)]$ complexes spectra. This appearance coincides to the bidentate attachment of sulphate group towards central atom[35]. While, the spectra of $[VO\ (CATP)(H_2O)]\ (SO_4)(H_2O)_2$ and $[VO(CATC)(H_2O)_2](SO_4)$ complexes, displayed only one band at; 1405 and 1357cm^{-1}, respectively. This agrees comfortably with stretching inside ionizable sulphate group. $\delta_r(H_2O)$ and $\delta_w(H_2O)$ bands have appeared in most complexes spectra. The bands were at; 755- 786 and 650 - 672 cm^{-1} ranges, respectively. A characteristic band attributing to ν(V=O) has clearly appeared in almost the same area for all complexes (≈1050 cm^{-1}); except for $[VO\ (CATP)(H_2O)](SO_4)(H_2O)_2$ (at 992 cm^{-1}). This band position is strongly coherent to the number of bonds surround vanadium atom [36]. The exception of such complex may refer to differ coordination number (five) from the rest (six). New ν(V-O), ν(V-N) and ν(V-S) bands, shined at low wavenumber region, confirm the mode of bonding for traizoles versus VO(II) atom.

3.4. Electronic transition bands

Remarkable bands were grouped and displayed in Table 4. The spectra have been obtained in DMSO solvent by influence of Uv-Vis spectral region. π → π* and n→ π* transitions were the significant intra ligand transitions observed at; 47619.05- 50505.0 and 32258.06-34013.61cm^{-1} attributing to free traizole derivatives, respectively[37]. The high degree of chromophoric conjugation inside the molecules influences on the deep colors observed attached with charge transfer inside the free compounds. Most of these bands suffer noticeable shift in the complexes spectra, which may belong to coordinating groups, which orients to facilitating electronic transition pathway inside groups. Also, in all complexes except for $[VO(CATP)(H_2O)](SO_4)(H_2O)_2$, significant d-d transition bands were recorded at 11261-11494 and 14260- 15356 cm^{-1} ranges. According to molecular orbital theory, these bands assign for; $^2B_2g \rightarrow {}^2Eg$ and $^2B_2g \rightarrow {}^2B_1g$ in distorted octahedral geometry (Fig. 3). In the environment of C4v symmetry, the ground state is a singlet orbital and the one electron in d is in non-bonding type (dxy, ^2B_2g). The crystal field stabilization energy values (Dq) were calculated based on; $^2B_2g \rightarrow {}^2B_1g$ (υ_1) = 10Dq relation, and the values agree with known reported [38]. As we know that, the value of crystal field stabilization energy, is fully matching with the first transitional band value (υ_1) through the former equation. While, the rest complex displayed 18182 and 19347 cm^{-1} bands, which they attributing to $^2B_2 \rightarrow {}^2E$ and $^2B_2 \rightarrow {}^2B_1$ transition, respectively in square-pyramidal geometry (Fig. 4). Also, new charge transfer bands were estimated assign for O→ V, N→V and S→ V, respectively.

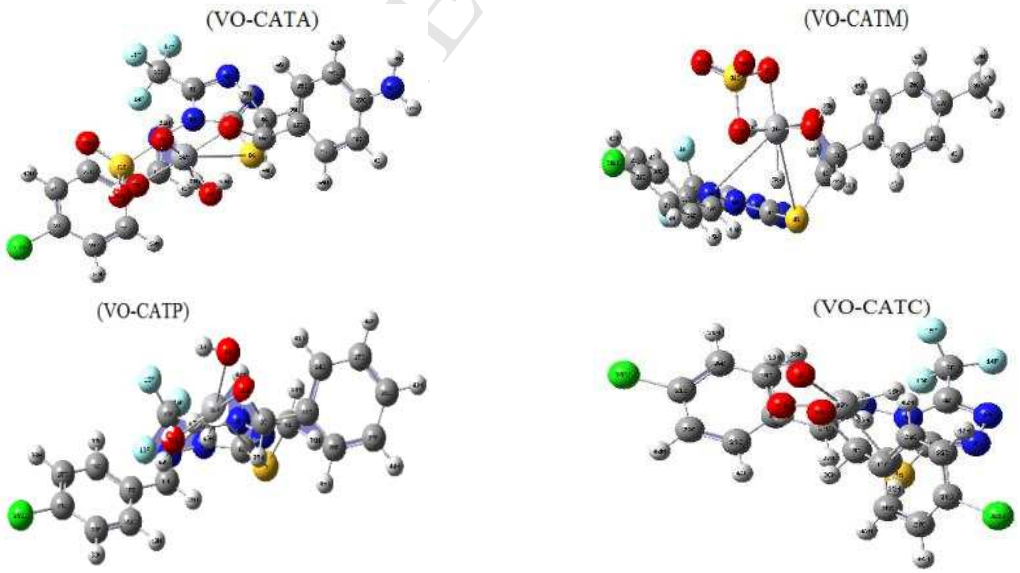

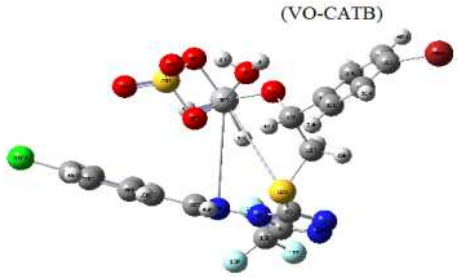

Fig. 3. Optimized structures of VO(II) -traizole complexes

3.5. Mass spectra

Mass spectral analysis is considered the most essential tool, which used to assert the molecular formula, particularly with failure in isolating single crystal for any synthesis. Figure 5 displays MS spectra of two selected complexes; $[VO(CATP)(H_2O)](SO_4)(H_2O)_2$ and $[VOSO_4(CATB)]$. The spectrum of $[VO(CATP)(H_2O)](SO_4)(H_2O)_2$ complex shows; molecular ion peak at m/z = 606.91 (I= 2.97, calcd. 641.86) which may attribute to M^+-$2H_2O$. The dehydration process may occur during the vaporization of complex before its bombardment by electron beam. The successive fragmentation stages were displayed in **scheme 3**, which were ended by a peak at m/z = 43.06 (I = 38.85), which agrees with vanadium isotope. The spectrum of $[VOSO_4(CATB)]H_2O$ complex shows a molecular ion peak at m/z = 666.22 (I= 2.28, calcd 666.72). The ion peak is approximately coinciding to M^+. This little difference, is logical with the presence of chlorine atom or vanadium, which are known by their isotopic nature. Also, successive fragmentation process, was ended by a peak at m/z= 45.03(I= 10.66), which strongly agrees with vanadium isotope [39].

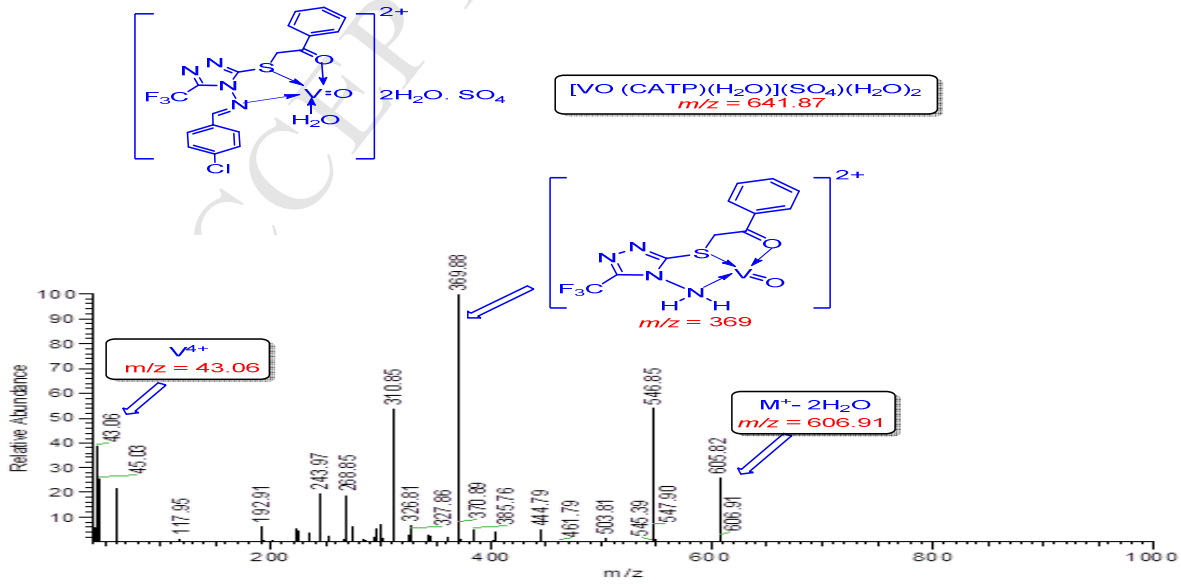

Scheme. 3. The proposed fragmentation for $[VO(CATP)(H_2O)](SO_4)(H_2O)_2$ complex

3.6. EPR study

EPR spectral analysis were conducted at; υ = 9.435 GHz, upon four investigated complexes. The binding nature around VO(II) atom for complexes, can be obtained through computing Hamiltonian parameters(Table 5)[40]. Vanadyl ion represents d^1 systems, which transfer electron to D^2 in distorted geometry. This electron occupies t_2g orbitals, which corresponding to T_2g (ground state term). Eight hyperfine splitting lines, is the expected appearance of VO(II) spectra(*I = 7/2*). In C_{4v} symmetry, two sets of lines (eight lines) were predicted, while in symmetry of C_{2v}, the expectation for three sets of eight lines. But, the spectra of the complexes have been appeared with poor resolution and highly smooth (Fig. 6). This may refer to high d-d interaction between neighboring centers which affects directly on degree of lines splitting. $g_{//} < g_{\perp} < g_e$ shows the presence of un-paired electron in $d_{xy,}$ which attributing to tetragonal geometry. Isotropic and anisotropic parameters were calculated by; $A_o = (A_{11}+2A_{\perp})/3$ and $g_o = (g_{11}+ 2g_{\perp})/3$ relations [41].This parameters display high degree of deviation from free electron value (g_e = 2.0023). These parameters (A and g) point to distorted tetragonal geometry. The G values calculated from this relation; $G = (g_{//}-2.0023)/(g_{\perp}- 2.0023) = 4$, suffer high reduction except for square-pyramidal complex. This reduction is corresponding to high-exchange interaction between vanadium centers in neighboring particles. Also, this high interaction orients to the cause for smoothly curves obtained, which is considered the main reason prohibiting the resolution for hyperfine splitting [42]. MO indexes (β^2 and α^2) have been calculated using known equations[43].The values calculated reflect the highly ionic feature of in plane- σ- or π- bonding around central atom[41]. The dipole term (p) values have been calculated by known relation[44] after using the anisotropic parameters ($A_{//}$ and $A_{\perp}$)by negative values. The values agree with that known for VO(II) ion. Also, the Fermi-contact term (K) values, calculated [45], point to the relatively high magnetic interaction of single electron with the atomic nucleus. The ability for minimizing $A_{//}$ value against $g_{//}$ value, is called a tetrahedral distortion index ($f = g_{//}/A_{//}$)[41] which clarify the high distortion of all complexes.

3.7. XRD and SEM analysis

XRD patterns have been obtained at $10^{\circ} < 2\theta < 90^{\circ}$ range (Fig. 7 &2S). This analysis gave a good view about the crystal lattice dynamics. Also, assert on purity of tested compounds from starting materials using known methods [46].Only two patterns represent the nano-crystalline feature for

corresponding complexes; $[VOSO_4(CATM)]2H_2O$ (A) and $[VOSO_4(CATB)]$. While, the rest, which are treated in XRD study(four compounds), introduce patterns attributing to the amorphous feature. The crystallinity advantage, may reflect a perfect building for the atomic arrays in distinct layers, which facilitate calculating the crystal physical indexes. Using high intense peak, crystallite parameters; 2θ, d spacing, FWHM, relative intensity, particle sizes, crystal strain (ε) and dislocation density(δ) have been estimated (Table 6)using known equations[47].The crystallite sizes calculated fall comfortably in nanometer range. However, the amorphous advantage for other investigated may refer to the fast precipitation for such compounds which led to this irregularity in the arrangement of particles or atoms. The crystal strain and dislocation density are the two indexes throwing a light on the network dislocation. Their reduced values, point to high regularity in the crystal lattice of the two nano-complexes. SEM images (Fig. 3S) for all tested compounds were obtained after electron beam scanning for the solid surface. The topography, morphology and the microstructures of solid surfaces were mostly in rocky or fused shape except for two complexes (VO-CATM and VO-CATB). The crystallite surface of the two complexes, reflects a spherical particle shape. This agrees strongly with XRD patterns. Also, large variation between the free derivatives and their regarding complexes confirms the purity of VO(II) complexes from starting materials[48]. This relatively similar topography, may refer to extreme similarity of preparation conditions conducted. The XRD, SEM and vanadium content for oxides obtained from the calcinations for $[VOSO_4(CATM)]2H_2O$ and $[VOSO_4(CATB)]$ complexes, have been discussed. XRD pattern (Fig. 7) was matched with other standard pattern, which likely to be V_2O_5 oxide. The distinctive nanometer size calculated, (Table 6) the high strain and dislocation inside the crystal, all of them may assist its catalytic activity. Also, SEM image display a regular morphology completely different from that of original complex. As well as the vanadium content was determined after complete digestion for 0.02g (in conc HNO_3), using a known complexometric method [14] to verify the molecular formula suggested.

3.8. TGA analysis

Assumptions for degradation technique regarding triazole derivatives and their VO(II) complexes have been displayed in Table 1S. The compounds have been heated (20-900^oC range) at constant heating rate ($10^oC\ min^{-1}$) under nitrogen. TGA curves for traizole derivatives displayed three to four decomposition stages except for 6e (CATB) compound degraded in two stages. The organic compounds displayed a complete degradation under heating system without residue, except for 6e compound, leave four carbon atoms. Up to 450 ^oC was sufficient for complete vaporization for most organic compounds, which is logically known. TGA curves for VO(II)-traizole complexes represented

three to four degradation stages upon all thermally unstable complexes except for [$VOSO_4$(CATB)]. The mechanism of degradation was proposed separately, for each complex, depending on the structural form of it. The lower thermal stability is the main feature observed for all complexes except for [$VOSO_4$(CATA)] and [VO(CATC)$(H_2O)_2$](SO_4) complexes. This exception due to the absence of crystal water molecules, which conducts to easiest degradation. Up to 800^oC was sufficient for complete distortion of coordination sphere, leaving VO_2, which mainly polluted by carbon atoms still. The plausible degradation scheme, displays an adequate conformity, about; found/ calculated mass losses proposed in each stage.

3.9. Computational study

3.9.1. Kinetics

The kinetics upon DTG curves have been investigated for traizole derivatives and their complexes. Only one step (1^{st}, 2^{ed} or 3^{rd}) was chosen for calculating thermodynamic parameters (E, ΔH, ΔS and ΔG). The selected stage has a moderate sharpness and definite borders to facilitate determining fraction decompose (α) versus temperature. Coats–Redfern[17] and Horowitz–Metzger equations[22] were the two comparative methods used. The kinetics, over all degradation process, give a great impact about the strength of whole chemical building. Also, clarify the impact of metal atoms inserted in organic compounds upon the thermal feature of chemical structure. Over extracted plots (Figs. 4S&5S) and applying the two methods, thermodynamic parameters have been calculated (Table 2S). $\Delta H = E + PV$, $\Delta G = \Delta H - T\Delta S$ and $\Delta S^* = R \ln (Ah/K_bT_S)$ were the equations used for calculation. Whereas; k_B and h are the Boltzmann and Plank's constants, respectively. T_s is the midpoint temperature for the selected stage. The data shown the following essential notices; i) high activation energy values were generally recorded for complexes in comparing to relative free ligands. This may be explained based on thermal stability for coordinating organic compounds. ii) Negative signs for ΔS values reflect the degree of randomness for the complexes versus to original ligands. iii) The positive Δ*H* values introduces endothermic feature for all decomposition stages. iv) Δ*G* values were generally raise in complexes which attached to the values of ΔH and ΔS.

3.9.2. DFT/B3LYP method

The best structural forms for organic derivatives (Fig. 1) and their VO(II) complexes (Fig. 3) were extracted, applying Gaussian09 program. DFT/B3LYP was the suitable method used for optimization process using 6-31G base set [49,a&b]. The resulted files (log and chk) were visualized over program screen to extract essential physical parameters. E_{HOMO}, E_{LUMO} and ΔE(energy gap) were

the first essential indexes computing belonging to frontier levels. Such level energy values, have a significant impact on the general characteristics for compounds. The frontiers images (HOMO & LUMO) for all treated compounds, were displayed in Figs 8 & 6S. The HOMO levels in all traizole ligands, appeared concentrated along traizole ring as well as aromatic-p-substituent moiety. However, the LUMO levels appeared in the opposite site beside the traizole ring also. This represent, a high electron density over the bound space, which is logical with the presence of intensive donor atoms in this area of the compounds. Moreover, HOMO & LUMO images upon VO(II) complexes, displayed divers features belonging to the distribution of such levels around the central atom. HOMO & LUMO images reflect a high concentration around the coordinating atoms, surround vanadyl. Moreover, the LUMO levels more prolonged over the whole molecules, in comparing to HOMO levels.

3.9.2.1. Computed physical parameters

Electronegativity (χ), chemical potential (μ), global hardness (η), global softness (S), global electrophilicity index (ω) and absolute softness (ϭ) were the estimated parameters using known equations[26,27]. The values of these physical parameters (Table 7), were obtained based on frontiers energy gap (E_{LUMO}-E_{HOMO}). Electrophilicity index (ω) is the guide for toxicity and reactivity of tested compound. As, a measure for the ability of acquiring electrons from surrounding. With regarding to traizole derivatives, a significant difference was recorded over all estimated physical parameters, which may attribute to the impact of *p*- substituents. Regarding to complexes, essential notices were summarized as follow; i) the complexes showed high electrophilicity values relative to their corresponding ligands. VO(II)-CATM has the superiority in attributing to such index. ii) Global hardness (η) and global softness (S), are two faces for the same coin, introduces the degree of flexibility for structural form, which excellence with complexes[50,51]. iii) The ΔE(energy gap) values in VO(II) complexes, suffer a significant minimization, relative to original derivatives. This points to the influence of metal atom in the molecular orbital diagrams inside the molecules. iv) Enhanced biological feature for complexes, is strongly attached with their absolute softness (ϭ) values, which are clearly rose beside, their reduced energy gaps [52]. According to numbering scheme, other important characteristics were gathered from log files and showed in Table 8. Charges over coordinating atoms (S, N and O) were extracted for the free traizole derivatives and their corresponding complexes. Regarding to free traizole derivatives, the charges over these chosen atoms reveal a suitable variation, which assure on the influence of p-substituents on the electron density upon a whole compound. These charges suffer a significant reduction after complexation process. The ionic feature of new coordinating bonds can be concluded attributing to vanadium charge which mostly affected by a strong

charge transfer (L→ V). The minimization for heat of formation in coincides to complex formation, is an indicator for high stability of formed complexes. The increase of dipole moments, which is coherently with the complexation, reflect the impact of metal insertion on the overall electron density. Regarding to VO(II) complexes, unsteady oscillator strength features in comparing to free ligand, may be attributing to variable crowding surround central atom[53].

3.9.3. QSAR parameters

Quantitative structure–property relationships (QSAR) were estimated (Table 9) upon optimized structures from applying HyperChem(8.1) program. Surface area values clarify increasing in complexes compared to original ligands, which considered logically after complexation. Partition coefficient (log P) values, appeared reduced in VO(II) complexes, specifically with VO(II)-CATA and VO(II)-CATB. This points to the high biological feature which may be expected from such two complexes [54].While, the reactivity and polarizability values for VO(II)-CATM and VO(II)-CATB the complexes, showed a distinguish escalating feature from original ligands. These parameters likelihood the enhancement for whole characteristics. The reactivity, polarizability and crystallite size were the significant characteristic for choosing the complexes suitable in catalytic application.

3.9.4. Molecular Docking study

This computational study concerning to the degree of inhibition for the docked organic compound and protein of pathogen cells. This is considered the pre-test in drug designing. The obtained interaction data were displayed in Table 10. Each VO(II) complex was treated using MOE module versus 2hio DNA- protein, to conduct the inhibition view against infected cell acid[29,30]. The results appeared discriminated binding scores, which close to lower binding mode except for VO(II)-6d complex (Fig. 9). The ionic binding is the main type of interaction between ligand and receptor. This may refer to ionic characteristic of most complexes as well as enriched dipole feature over intensive functional-groups. While the other complexes were varied dramatically between moderate to nil binding mode (Figs 7S &8S). In general the complexes herein are not likely to be the target orients to 2hio protein receptor of infected cell-DNA, which directed us to another application pathway.

3.10. The catalytic application

The synthesis of biodiesel from waste cooking oil is major interest in this study. As we reported previously, that the cause for this choice is the unsafe process which mostly utilized in previous researches [55]. Formerly reported in the literature, the main catalyst used was CaO, which known by

its high reactivity and several requirements, must be taken in consideration, to achieve the process with adequate-safety. Here and regarding the safety of our proposed process, may be considered a successful alternative-process for biodiesel synthesis. [$VOSO_4$(CATB)] complex, was the selected one for this application based on its distinguish capacity as; surface area, reactivity, polarizability, nano-crystallinity, spherical particulate and thermal stability. These features may lead to significant impact on its catalytic behavior in preparing such economic product. Moreover, the calcinations techniques was applied upon the complex through the complete oxidation in open air and followed by ignition oven(650 ^{o}C). Yellow powdered oxide was obtained and fully characterized by; XRD, SEM and vanadium content. XRD and SEM introduces patterns coincide to that attributing to V_2O_5 oxide in its nano-sized spherical particles. Also, the evaluation for vanadium content asserts the formula proposed. The sunflower waste oil (WO) has been used for biodiesel synthesis in heterogeneous catalytic process (Figs. 10&10S). It was known that, this oil mainly consists of oleic acid as well as other fatty acids. Trans- esterification process (Scheme 3) has been tracked upon two comparative catalysts (complex, oxide), which they implemented at the same conditions [56,57].The oxide catalyst produced biodiesel, by a limited yield although its normal physical properties. Density, viscosity and cloud point were the physical parameters estimated(Table 3S) for synthesized biodiesel and have been compared with that for ASTM-6751 Biodiesel (reference)[58-60].Finally, the process utilizing the complex displayed that, the complex plays a best desired role in biodiesel synthesis at record time compared to oxide. This may refer to the promising features recorded for the complex from various physical investigations among experimental / theoretical techniques.

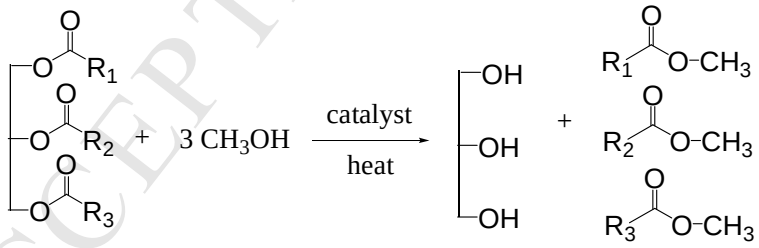

Scheme. 3. The transestrification of the waste oil to biodiesel

4. CONCLUSIONS

Novel VO(II)-traizole complexes, were prepared and fully characterized. Spectral and analytical data confirmed the molecular and structural formulae for all new synthesis. The obtained mononuclear complexes were appeared mainly in octahedral geometry. This proposal was confirmed by UV-Vis and ESR spectral data. The conformational study was implemented to verify the structural formulae proposed. Such, which mainly depends on the distribution of coordinating functional-groups, that basically obtained from optimization process. While, the molecular docking study was executed

by MOE module, to predict the biological activity of new complexes, before practical application. The absence of significant biological activity, which concluded from docking process as a preliminary step in drug designing, this orients us for another field of application, as catalysis. After that, distinguish properties of VO(II)-CATB complex motivate to be implemented in catalytic application. This study interested in biodiesel synthesis from cooking waste oils (WO). Moreover, the oxide of chosen complex, which obtained after calcinations (V_2O_5), was also utilized from comparative point of view to introduce the best. The complex revealed superiority in biodiesel-synthesis in comparing to its calcinations-oxide. Distinct physical parameters estimated for synthesized biodiesel, were compatible with standard values. The main advantage of our experiment lies in its safety and economic validity, in comparing to others previously reported.

ACKNOWLEDGEMENTS

Prof. Nashwa El-Metwaly and co-authors would like to thank Deanship of Scientific Research at Umm Al-Qura University (project ID: 17-SCI-1-03-0001) for the financial support to this research extracted from the project.

REFERENCES

[1] S.J. Yoo, H. Lee, B. Veriansyah, J. Kim, J. Kim, Y. Lee. Synthesis of biodiesel from rapeseed oil using supercritical methanol with metal oxide catalysts. Bioresource Technology 101 (2010) 8686–8689.

[2] C.-Y. Lin, H.-A. Lin, L.-B. Hung, Fuel structure and properties of biodiesel produced by the peroxidation process. Fuel, 85 (2006) 1743–1749.

[3] C. Pastore, A. Lopez, V. Lotito, G. Mascolo. Biodiesel from dewatered wastewater sludge: A two-step process for a more advantageous production. Chemosphere, 92 (2012) 667-673.

[4] M. Pirouzmand, M. M. Anakhatoon, Z. Ghasemi, One-step biodiesel production from waste cooking oils over metal incorporated MCM-41; positive effect of template. Fuel, 216 (2018) 296-300.

[5] B.R. Vahid, N. Saghatoleslami, H. Nayebzadeh, J. Toghiani, Effect of alumina loading on the properties and activity of SO42−/ZrO2 for biodiesel production: Process optimization via response surface methodology. J. Taiwan Institute Chem. Eng., 83 (2018) 115-123.

[6] B. Peng, Q. Shu, J. Wang, G. Wang, D. Wang, M. Han, Biodiesel production from waste oil feedstocks by solid acid catalysis. Process Safety and Environment Protection, 86 (2008)

441-447.

[7] A.B. Fadhil, E.T.B. Al-Tikrity, M.A. Albadree, Biodiesel production from mixed non-edible oils, castor seed oil and waste fish oil. Fuel, 210 (2017) 721-728.

[8] M. Weyand, H. J. Hecht, M. Kiess, M.F. Liaud, H. Vilter, D. Schomburg, X-ray Structure Determination of a Vanadium dependent Haloperoxidase from Ascophyllum nodosum at 2.0 AÊ Resolution J. Mol. Biol. 293 (1999) 595-611.

[9] J. N. Carter-Franklin, J. D. Parrish, R.A. Tchirret-Guth, R. D. Little, A. Butler, Vanadium haloperoxidase-catalyzed bromination and cyclization of terpenes. J. Am. Chem. Soc. 125 (2003) 3688-3689.

[10] D. Rehder, Bioinorganic Vanadium Chemistry, John Wiley & Sons, New York, (2008).

[11] C. Bolm, Vanadium-catalyzed Asymmetric Oxidations. Coord. Chem. Rev., 237(**2003**) 245-256.

[12] A. Ayati, S. Emami, A. Foroumadi, *The importance of* triazole *scaffold in the development* of anticonvulsant *agents*, Eur. J. Med. Chem., 109 (2016) 380-392.

[13] M. Chen, X. Wang, S. Wang, Y. Feng, F. Chen, C. Yang. Synthesis, characterization and fungicidal activities of novel fluorinated 3,5-disubstituted-4*H*-1,2,4-triazol-4-amines. J. Fluorine Chem., 135(2012) 323-329.

[14] A. I. Vogel. Text Book Of quantitative Inorganic Analysis Longman, London (1986).

[15] G.A. Bain, J.F. Berry, Diamagnetic Corrections and Pascal's Constants. Chem. Educ., 85 (2008) 532-536.

[16] E. S. Freeman, B. Carroll, The Application of Thermoanalytical Techniques to Reaction Kinetics: The Thermogravimetric Evaluation of the Kinetics of the Decomposition of Calcium Oxalate Monohydrate. J. Phys.Chem., 62 (1958) 394-397.

[17] W. Coats, J. P. Redfern, Kinetic Parameters from Thermogravimetric Data. Nature, 201 (1964) 68-69.

[18] T. Ozawa, A New Method of Analyzing Thermogravimetric Data. Bull. Chem. Sot. Japan., 38 (1965) 1881-1886.

[19] W. W. Wendlandt, Thermal Methods of Analysis, New York, Wiley (1974).

[20] J. H. F. Flynn, L. A. Wall, General Treatment of the Thermogravimetry of Polymers. J. Res. Natl. Bur. Stand. A. 70 (1966) 487-523.

[21] P. Kofstad, Oxidation of Metals: Determination of Activation Energies. Nature, 179 (1957) 1362-1363.

[22] H. W. Horowitz, G. A.Metzger, A New Analysis of Thermogravimetric Traces. Anal Chem., 35

(1963) 1464-1468.

[23] X. Wu. A. K. Ray, Density-functional study of water adsorption on the PuO_2(110) surface. Phys. Rev. B., 65 (2002) 85403-7.

[24] M. J. Frisch, et al., Gaussian 09, Revision D, Gaussian, Inc., Wallingford, CT, (2010).

[25] R. Dennington, T. Keith , J. Millam .Gauss View, Version 4.1.2, SemichemInc, Shawnee Mission, KS, (2007).

[26] U. El-Ayaan, N. M. El-Metwally, M. M.Youssef, S. A. A. El Bialy, Perchlorate mixed–ligand copper(II) complexes of β-diketone and ethylene diamine derivatives: Thermal, spectroscopic and biochemical studies. Spectrochim. Acta, Part A, 68 (2007) 1278-1286.

[27] R. K. Ray, G. R. Kauffman, EPR Spectra and covalency of bis(amidinourea/*O*-alkyl-1-amidinourea)copper(II) complexes Part II. Properties of the CuN_4^{2-} chromophore. Inorg. Chem. Acta, 173 (1990) 207-214.

[28] M. M. Al-Iede, J. Karpelowsky, D.A. Fitzgerald , Recurrent diaphragmatic hernia: modifiable and non-modifiable risk factors Pediatr Pulmonol, (2015).

[29] K. H. Mashat, B. A. Babgi, M. A. Hussien, M. N. Arshad, M. H. Abdellattif, Synthesis, structures, DNA-binding and anticancer activities of some copper(I)-phosphine complexes. Polyhedron 158 (2019) 164–172.

[30] M. H. Abdellattif, M. A. Hussien, E. Alzahrani, New Approaches of 4-Aryl-2-Hydrazinothiazole derivatives, molecular docking, and biological evaluations, IJPSR, 9(12)(2018)1000-1019.

[31] V. Narula, M. F. Khan, A. Negi, S. Kalra, A. Thakur, S. Jain. Low temperature optimization of biodiesel production from algal oil using CaO and CaO/Al_2O_3 as catalyst by the application of response surface methodology. Energy, 140 (2017) 879-884.

[32] J. F. Puna, J. F. Gomes, J. C. Bordado, M. Joana, N. Correia, A. Paula, S. Dias. Biodiesel production over lithium modified lime catalysts: Activity and deactivation. Applied Catalysis A: General, 470 (2014) 451-457.

[33] V.B. Veljković, O.S. Stamenković, Z.B. Todorović, M.L. Lazić, D.U. Skala, Kinetics of sunflower oil methanolysis catalyzed by calcium oxide. Fuel, 88 (2009) 1554-1562.

[34] W.J. Geary, The use of conductivity measurements in organic solvents for the characterisation of coordination compounds. J. Coord. Chem. Rev. 7 (1971) 81-122.

[35] N. M. El-Metwaly, R. M. El-shazly, I. M. Gabr, A. A. El-Asmy, Physical and spectroscopic studies on novel vanadyl complexes of some substituted thiosemicarbazides. Spectrochim. Acta, 61 (2005) 1113-1119.

[36] K. S. Abu-Melhaa, N. M. El-Metwally, Spectral and thermal studies for some transition metal complexes of bis(benzylthiocarbohydrazone) focusing on EPR study for Cu(II) and VO^{2+}. Spectrochim. Acta, Part A, 70 (2008) 277-283.

[37] A.A. Abou-Hussen, N.M. El-Metwaly, E.M. Saad, A.A. El-Asmy, Spectral, magnetic, thermal and electrochemical studies on phthaloyl bis(thiosemicarbazide) complexes. J. Coord. Chem. 58 (2005) 1735-1749.

[38] A. B. P. Lever Inorganic Electronic Spectroscopy, Elsevier, Amsterdam (1986).

[39] M. S. Refat, N. M. El-Metwaly, Structure and vibrational spectroscopy investigation of 2-(4-chlorophenyliminomethyl)-8-hydroxyquinoline. Spectrochimica Acta Part A, 81 (2011) 215-256.

[40] E. Bagdatil, E. Altuntas, U. Sayin, Synthesis and structural characterization of new oxovanadium (IV) complexes derived from azo-5-pyrazolone with prospective medical importance. J. Mol. Struct. 1127 (2017) 653-661.

[41] H. Yokoi, A. W. Addison, Spectroscopic and redox properties of pseudotetrahedral copper(II) complexes. Their relation to copper proteins. Inorg. Chem. 16 (1977) 1341-1349.

[42] a) B. J. Hathaway, D.E. Billing. The electronic properties and stereochemistry of mono-nuclear complexes of the copper(II) ion. Coord. Chem. Rev., 5 (1970) 143-207, b) B. J. Hathaway, A new look at the stereochemistry and electronic properties of complexes of the copper(II) ion. Struct. Bonding (Berlin), 57 (1984) 55-118.

[43] T. M. Dunn, Spin-orbit coupling in the first and second transition series. Trans. Faraday Soc., 57 (1961) 1441-1444.

[44] B. R. Mc Garvey, The isotropic hyperfine interaction. J. Phys. Chem., 71 (1967) 51-67.

[45] M. Salagram, N. Satyanarayana , S. Radhakrishna. Semi-empirical evaluation of molecular-orbital parameters, and spin—orbit, dipolar and fermi-contact terms of VO^{2+} ion in lattices. Polyhedron, 5 (1986) 1171-1181.

[46] B. D. Cullity, Elements of X –ray diffraction. second ed., Addison –Wesley Inc., (1993).

[47] S. Velumani, X. Mathew, P.J. Sebastian, Sa.K. Narayandass, D. Mangalaraj, Structural and optical properties of hot wall deposited CdSe thin films. Sol. Cells, 76 (2003) 347-358.

[48] J. S. Ritch, T. Chivers, K. Ahmad, M. Afzaal, P. O. Brien, Synthesis, Structures, and Multinuclear NMR Spectra of Tin(II) and Lead(II) Complexes of Tellurium-Containing Imidodiphosphinate Ligands: Preparation of Two Morphologies of Phase-Pure PbTe from a Single-Source Precursor. *Inorg. Chem.*, 49 (2010) 1198-1205; T. Mokari, M. Zhang, P. Yang,

Shape, Size, and Assembly Control of PbTe Nanocrystals. *J. Am. Chem. Soc*. *129* (2007) 9864-9865; J. J. Urban, D. V. Talapin, E. V. Shevchenko, C. B. Murray, Self-Assembly of PbTe Quantum Dots into Nanocrystal Superlattices and Glassy Films. J. Am. Chem. Soc., 128 (2006) 3248-3255.

[49] 1- A) I. Althagafi, M. G Elghalban, F. Saad, J. H Al-Fahemi, N. M El-Metwaly, S. Bondock, L. Almazroai, K. A Saleh, G. A Al-Hazmi, Spectral characterization, CT-DNA binding, DFT/B3LYP, molecular docking and antitumor studies for new nano-sized VO (II)-hydrazonoyl complexes, J. of Mol. Liq., 242(2017)662; B) G. A Al-Hazmi, K. S Abou-Melha, **N. M El-Metwaly**, K. A Saleh , Synthesis of Novel VO (II)-Perimidine Complexes: Spectral, Computational, and Antitumor Studies, , Bioinorganic Chemistry and ApplicationsVolume 2018(2018) Article number 7176040

[50] R. C. Chikate, S. B. padhye, Transition metal quinone–thiosemicarbazone complexes 2: Magnetism, ESR and redox behavior of iron (II), iron (III), cobalt (II) and copper (II) complexes of 2-thiosemicarbazido-1,4-naphthoquinone. Polyhedron, 24 (2005) 1689-1700.

[51] H. Allal, Y. Belhocine, E. Zouaoui. Computational study of some thiophene derivatives as aluminium corrosion inhibitors. J. Mol. Liq., 265 (2018) 668-678.

[52] I. Fleming, Frontier Orbital's and Organic Chemical Reactions, Wiley, London, (1976).

[53] S. K. Tripathi, R. Muttineni, S. K. Singh, Extra precision docking, free energy calculation and molecular dynamics simulation studies of CDK2 inhibitors. J. Theor. Biol., 334 (2013) 87-100.

[54] F. A. Saad, J. H. Al-Fahemi, H. El-Ghamry, A. M. Khedr, M. G. Elghalban, N. M. El-Metwaly, Elaborated spectral, modeling, QSAR, docking, thermal, antimicrobial and anticancer activity studies for new nanosized metal ion complexes derived from sulfamerazine azodye. J. Therm. Anal. Calorim., 13 (2018), 1249-1267.

[55] Z. Kesic, I. Lukic, M. Zdujic, L. Mojovic and D. Skala, Calcium Oxide Based Catalysts for Biodiesel production(Review), Chem. Ind. Chem. Eng. Q . 22 (4) 391−408 (2016)

[56] N. Terakado, S. Shintani, Y. Nakahara, Expression of Cu,Zn-SOD, Mn-SOD and GST-pi in oral cancer treated with preoperative radiation therapy. Oncol Rep, 7 (2000) 1113-1120.

[57] V. Singh, M. Yadav, Y. C. Sharma. Effect of co-solvent on biodiesel production using calcium aluminium oxide as a reusable catalyst and waste vegetable oil. Fuel, 203 (2017) 360-369.

[58] I. B. Banković–Ilić, M. R. Miladinović, O. S. Stamenković, V. B. Veljković, Application of nano CaO–based catalysts in biodiesel synthesis. Renewable and Sustainable Energy

Reviews, 72 (2017) 746-760.

[59] N.A. Negma, G.H. Sayed, O.I. Habiba, F.Z. Yehia , E.A. Mohamed, Heterogeneous catalytic transformation of vegetable oils into biodiesel in one-step reaction using super acidic sulfonated modified mica catalyst. J. Molecular Liq., 237 (2017) 38-45.

[60] L.M. Correia, N.S. Campelo, D.S. Novaes, C.L. Cavalcante Jr, J.A. Cecilia, E. Rodríguez-Castellón, R.S. Vieira, Characterization and application of dolomite as catalytic precursor for canola and sunflower oils for biodiesel production. Chem. Eng. J., 269 (2015) 35-43.

Table 1 Analytical data of triazole derivatives (**6a-e**) and their VO(II) complexes

Compounds (Empirical formula)	Λ_m, Ohm^{-1}cm^2 mol^{-1}	Color	Elemental analysis (%) Calcd (Found)					
			C	H	N	Cl	S	V
1) ($C_{18}H_{13}ClF_3N_5OS$)(CATA,**6a**)(439.84)	---	Yellow	49.15(49.14)	2.98(2.96)	15.92(15.92)	8.06(8.05)	7.29(7.29)	------
2)[VO SO_4(CATA)](602.84)	6.30	Olive green	35.86(35.85)	2.17(2.15)	11.62(11.60)	5.88(5.89)	10.64(10.62)	8.45(8.41)
3) ($C_{19}H_{14}ClF_3N_4OS$)(CATM,**6b**)(438.85)	---	Brown	52.00(52.05)	3.21(3.20)	12.77(12.78)	8.08(8.08)	7.31(7.30)	------
4)[VO SO_4(CATM)]2H_2O(637.88)	5.41	Olive green	35.78(35.79)	2.84(2.82)	8.78(8.77)	5.56(5.53)	10.05(10.10)	7.99(8.02)
5) ($C_{18}H_{12}ClF_3N_4OS$)(CATP,**6c**)(424.82)	---	Brown	50.89(51.02)	2.85(2.84)	13.19(13.21)	8.35(8.36)	7.55(7.57)	------
6)[VO (CATP)(H_2O)](SO_4)(H_2O)$_2$(641.86)	51.75	Brown	33.68(33.65)	2.83(2.87)	8.73(8.76)	5.52(5.55)	9.99(10.10)	7.94(7.95)
7) ($C_{18}H_{11}Cl_2F_3N_4OS$)(CATC,**6d**)(459.27)	---	Faint yellow	47.07(47.02)	2.41(2.40)	12.20(12.18)	15.44(15.41)	6.98(695)	------
8)[VO (CATC)(H_2O)$_2$](SO_4)(658.30)	44.63	Olive green	32.84(32.85)	2.30(2.28)	8.51(8.47)	10.77(10.76)	9.74(9.70)	7.74(7.73)
9)($C_{18}H_{11}BrClF_3N_4OS$)(CATB,**6e**)(503.72)	---	Yellow	42.92(42.92)	2.20(2.19)	11.12(11.12)	Cannot determined	6.37(6.36)	------
10)[VO SO_4(CATB)](666.72)	5.81	Olive green	32.43(32.56)	1.66(1.69)	8.40(8.39)	Cannot determined	9.60(9.57)	7.64(7.63)

Table 2 ^{1}H, ^{13}CNMR data for triazole derivatives (**6a-e**)

Compounds	^{1}H NMR	^{13}C NMR
6a, CATA	2.14 (s,2H, NH_2), 4.80 (s,2H, CH_2), 6.75-8.20 (m, 8H, Ar-H), 8.21 (s, 1H, N=CH).	41.68 (CH_2), [114.28, 121.84, 129.11, 129.55, 130.17, 130.93, 133.60, 134.02, 139.30, 142.53, 148.50, 160.39(Ar-C)], 196.50 (C=O)
6b, CATM	1.60 (s,3H, CH_3), 3.74 (s, 2H, CH_2), 7.30-8.02 (m, 8H, Ar-H), 8.64 (s, 1H, N=CH).	38.28 (CH_3), 55.52 (CH_2), [128.13, 129.17, 129.49, 129.76, 129.90, 130.14, 132.11, 132.43, 135.27, 135.60, 142.11, 142.80 (Ar-C)], 194.37 (C=O)
6c, CATP	4.12 (s,2H, CH_2), 7.16 (s,1H,N=CH) 7.19-7.85 (m, 9H, Ar-H).	45.05 (CH_2), [116.45, 119.14, 123.93, 125.90, 128.27, 128.36, 131.54, 135.94, 136.65, 140.54, 147.15, 155.07(Ar-C)], 190.86 (C=O)
6d, CATC	4.25 (s,2H, CH_2), 6.80-7.91(m, 9H, Ar-H) and N=CH).	48.0 (CH_2), [116.48, 119.17, 127.55, 127.70, 128.20, 128.93, 129.39, 129.72, 130.04, 143.82, 144.09, 154.97 (Ar-C)], 195.0 (C=O)
6e, CATB	4.03 (s,2H, CH_2), 7.29 (s,1H, N=CH), 6.73-7.95 (m, 8H, Ar-H).	49.20 (CH_2), [119.08, 127.94, 128.16, 128.93, 129.46, 130.16, 131.40, 132.68, 132.89, 143.40, 150.03, 154.07 (Ar-C)], 193.21 (C=O)

Table 3 Functional IR spectral bands (cm^{-1}) of triazole derivatives (6a-e) and their VO(II) complexes

Compounds	ν_{OH},ν_{CH-Ar}	$\nu_{C=O}$	$\nu_{C=N}$	ν_{C-S}	$\nu_{as(SO4)}$	$\nu_{s(SO4)}$	$\delta r(H_2O),\delta w(H_2O)$	$\nu_{V=O}$	ν_{M-O}	ν_{M-N}	ν_{M-S}
1) 6a, CATA	NH_2,3434,3152	1679	1603	679	----	----	----	----	----	----	----
2)[VO SO_4(CATA)]	3428,3153	1673	1591	653	1289	1158	----	1054	619	519	478
3) 6b, CATM	.....,3154	1687	1585	677	----	----	----	----	----	----	----
4)[VO SO_4(CATM)]2H_2O	B.C. 3428	1677	1576	666	1270	1160	755, 650	1049	610	554	470
5) 6c, CATP	.....,3187	1658	1572	687	----	----	----	----	----	----	----
6)[VO (CATP)(H_2O)](SO_4)(H_2O)$_2$	B.c. 3440	1615	1560	672	**ν,** ionic,1405		772, 672	992	593	B. c. 513	
7) 6d, CATC	.....,3151	1677	1567	680	----	----	----	----	----	----	----
8)[VO (CATC)(H_2O)$_2$] (SO_4)	3473,3152	1670	1533	657	**ν,** ionic, 1357		786, 660	1048	604	524	474
9)6e, CATB	....., 3064	1682	1569	655	----	----	----	----	----	----	----
10)[VO SO_4(CATB)]	-----	1671	1528	640	1252	1191	----	1058	606	542	470

B. c. Broad centered

Table 4 Electronic transition bands (cm^{-1}) for triazole derivatives (**6a-e**) and their VO(II) complexes

Compounds	**μ(eff) (B.M.)**	**Dq (cm^{-1})**	**d-d transition bands (cm^{-1})**	**Intraligand and charge transfer(cm^{-1})**	**Complex Geometry**
1) **6a**, CATA	-----		------	47619.05; 32258.06	------
2)[VO SO_4(CATA)]	1.73	1426	11261; 14260	50505.05; 34013.6; 25510.2	Octahedral
3) **6b**, CATM	-----		------	49504.95; 33783.78	------
4)[VO SO_4(CATM)]2H_2O	1.74	1535.6	11494; 15356	51546.39;34246.57; 32051.28; 24154.59	Octahedral
5) **6c**, CATP	-----		------	50505.05; 34013.60; 24038.46	------
6)[VO (CATP)(H_2O)](SO_4)(H_2O)$_2$	1.78		18182; 19347	49103.25; 33015.23; 25343.25	Square-pyramidal
7) **6d**, CATC	------		------	50505.05;34013.61	------
8)[VO (CATC)(H_2O)$_2$](SO_4)	1.78	1532.1	11494; 15321	50000.0; 34246.57; 24271.84	Octahedral
9)**6e**, CATB	----		------	49504.95; 34013.61	------
10)[VO SO_4(CATB)]	1.75	1487.3	11364; 14873	49456.74; 26178.01	Octahedral

Table 5 Spin – Hamiltonian parameters computed for most VO(II) complex (A and p x10^{-4})

Complex	$g_{//}$	$g_{\perp}$	g_o	A_{11}	f	$A_{\perp}$	A_o	G	p	k	α^2	β^2
2) [VO SO_4(CATA)]	1.927	1.971	1.956	161	119.69	62	95.00	2.406	115.09	0.779	1.102	1.530
4)[VO SO_4(CATM)]2H_2O	1.929	1.971	1.957	160	120.56	65	96.67	2.342	110.45	0.830	1.124	1.531
6)[VO (CATP)(H_2O)](SO_4)(H_2O)$_2$	1.920	1.979	1.959	175	109.71	73	107.00	3.532	----	----	1.964	1.090
8) [VO (CATC)(H_2O)$_2$](SO_4)	1.933	1.973	1.960	162	119.32	68	99.33	2.365	109.29	0.867	1.052	1.533

Table 6. XRD parameters for nano-crystalline complexes

Compounds	Size (Å)	2θ	Intensity	d-spacing (Å)	ε	δ(Å^{-2})	FWHM
1)[VO SO_4(CATM)]2H_2O	3.339	25.07	753.4	3.5492	0.1276	0.08969	0.4443
2)[$VOSO_4$(CATB)]	3.103	18.86	420.0	4.7015	0.1817	0.10386	0.4731
3) V_2O_5	1.462	26.25	240.3	6.7845	2.8016	0.4678	0.4286

Table 8. Estimated physical parameters upon optimized structures by DFT/B3LYP method

Compounds	E_H (eV)	EL (eV)	(EH - EL) (eV)	El-Eh	*x*(eV)	μ(eV)	η(eV)	S(eV-1)	ω(eV)	σ(eV)
CATA	-0.21524	-0.09152	-0.1237	0.12372	0.15338	-0.15338	0.06186	0.03093	0.190151	16.16553508
VO(II)+CATA	-0.24544	-0.15914	-0.0863	0.0863	0.20229	-0.20229	0.04315	0.021575	0.474174	23.17497103
CATM	-0.24915	-0.09103	-0.1581	0.15812	0.17009	-0.17009	0.07906	0.03953	0.182966	12.6486213
VO(II)+CATM	-0.26361	-0.18563	-0.078	0.07798	0.22462	-0.22462	0.03899	0.019495	0.647014	25.64760195
CATP	-0.25033	-0.08849	-0.1618	0.16184	0.16941	-0.16941	0.08092	0.04046	0.177334	12.35788433
VO(II)+CATP	-0.20102	-0.1285	-0.0725	0.07252	0.16476	-0.16476	0.03626	0.01813	0.374322	27.57859901
CATC	-0.26025	-0.10538	-0.1549	0.15487	0.182815	-0.18282	0.077435	0.038718	0.215802	12.91405695
VO(II)+CATC	-0.19613	-0.13965	-0.0565	0.05648	0.16789	-0.16789	0.02824	0.01412	0.499063	35.41076487
CATB	-0.25274	-0.09616	-0.1566	0.15658	0.17445	-0.17445	0.07829	0.039145	0.194359	12.77302337
VO(II)+CATB	-0.26764	-0.16272	-0.1049	0.10492	0.21518	-0.21518	0.05246	0.02623	0.441312	19.06214258

Table 9 Considerable bond lengths, charges, Heat of formation (E), dipole moment(D), oscillator strength(ʃ)and excitation energies(E)

Compounds	S^6 / S^7 (coordinated)	N^{15}/ N^{16} (coordinated)	O^9/ O^{10} coordinated)	V	E (A.U.)	D(Debye)	ʃ	E(nm)
CATA	0.442405	-0.150616	-0.409986	-------	-2200.10305276	4.3324	0.0003	403.84
VO(II)+CATA	/ 0.026146	/ 0.001056	/0.200855	-0.197636	-3920.26108263	18.1672	0.0004	11834.2
CATM	0.443330	-0.142443	-0.395659	-------	-2184.06749538	3.1809	0.0185	342.17
VO(II)+CATM	/ 0.090623	/ 0.004075	/ 0.330341	-0.280582	-3904.22467118	8.3523	0.0036	8988.13
CATP	0.445146	-0.132537	-0.394706	-------	-2144.75414290	3.1744	0.0316	335.04
VO(II)+CATP	/ 0.126080	/ -0.002343	/ -0.078191	1.700495	-3241.34103856	7.0427	0.0002	2125.97
CATC	0.397484	-0.110515	-0.327687	-------	-2604.73939397	3.5916	0.0074	351.01
VO(II)+CATC	/ 0.043118	/ 0.008932	/-0.003311	0.314163	-3700.44294622	6.6361	0.0015	5768.26
CATB	0.449863	-0.150324	-0.390935	-------	-4715.73185415	3.4109	0.0128	346.48
VO(II)+CATB	/ 0.100144	/ 0.039138	/ 0.250164	-0.056450	-6437.00965246	7.2977	0.0162	4807.21

Table 10 Computational QSAR parameters for optimized triazole derivatives and their VO(II) complexes

Function	6a	6b	6c	6d	6e	VO-CATA	VO-CATM	VO- CATP	VO-CATC	VO-CATB
Surface area (Approx) ($Å^2$)	574.23	611.51	568.37	602.71	614.09	583.08	610.77	562.93	600.48	603.09
Surface area (Grid) ($Å^2$)	655.29	663.22	638.97	658.00	679.00	672.13	683.11	642.41	667.81	697.01
Volume ($Å^3$)	1077.75	1097.92	1045.71	1088.84	1108.19	1198.82	1217.51	1113.25	1158.03	1238.13
Hydration energy(Kcal/mol)	-16.07	-9.72	-10.90	-10.45	-10.57	-26.40	-20.02	-24.85	-24.61	-18.10
Log P	2.73	4.60	4.45	4.23	4.50	1.23	3.10	2.57	2.35	1.86
Reactivity ($Å^3$)	114.32	115.06	110.77	115.49	118.31	129.09	129.82	117.28	121.99	133.20
Polarizability ($Å^3$)	40.58	41.06	39.22	41.15	41.85	42.08	43.56	39.72	41.65	43.49

Table 11 Interaction parameters for VO(II) complexes against calf thymus DNA (2hio) complexes

Complex	Ligand	Receptor	Interaction	Distance(Å)	E (Kcal/mol)	S(energy score)
VO(II)-6a	6-ring	N ARG 134 (C)	pi-H	4.67	-0.8	-6.3282
VO(II)-6b	F 27	NZ LYS 99 (A)	H-acceptor	3.04	-1.2	-5.5948
	C 30	NZ LYS 99 (A)	Ionic	3.13	-3.7	
VO(II)-6c	----	----	----	----	----	-6.1536
VO(II)-6d	O 8	OD2 ASP 68 (B)	Ionic	3.07	4.0	-6.3398
	S 11	OE2 GLU 71 (B)	Ionic	3.39	-2.3	
	N 28	OE1 GLU 71 (B)	Ionic	3.78	-1.0	
	N 28	OE2 GLU 71 (B)		3.39	-2.3	
VO(II)-6e	----	----	----	----	----	-6.2867

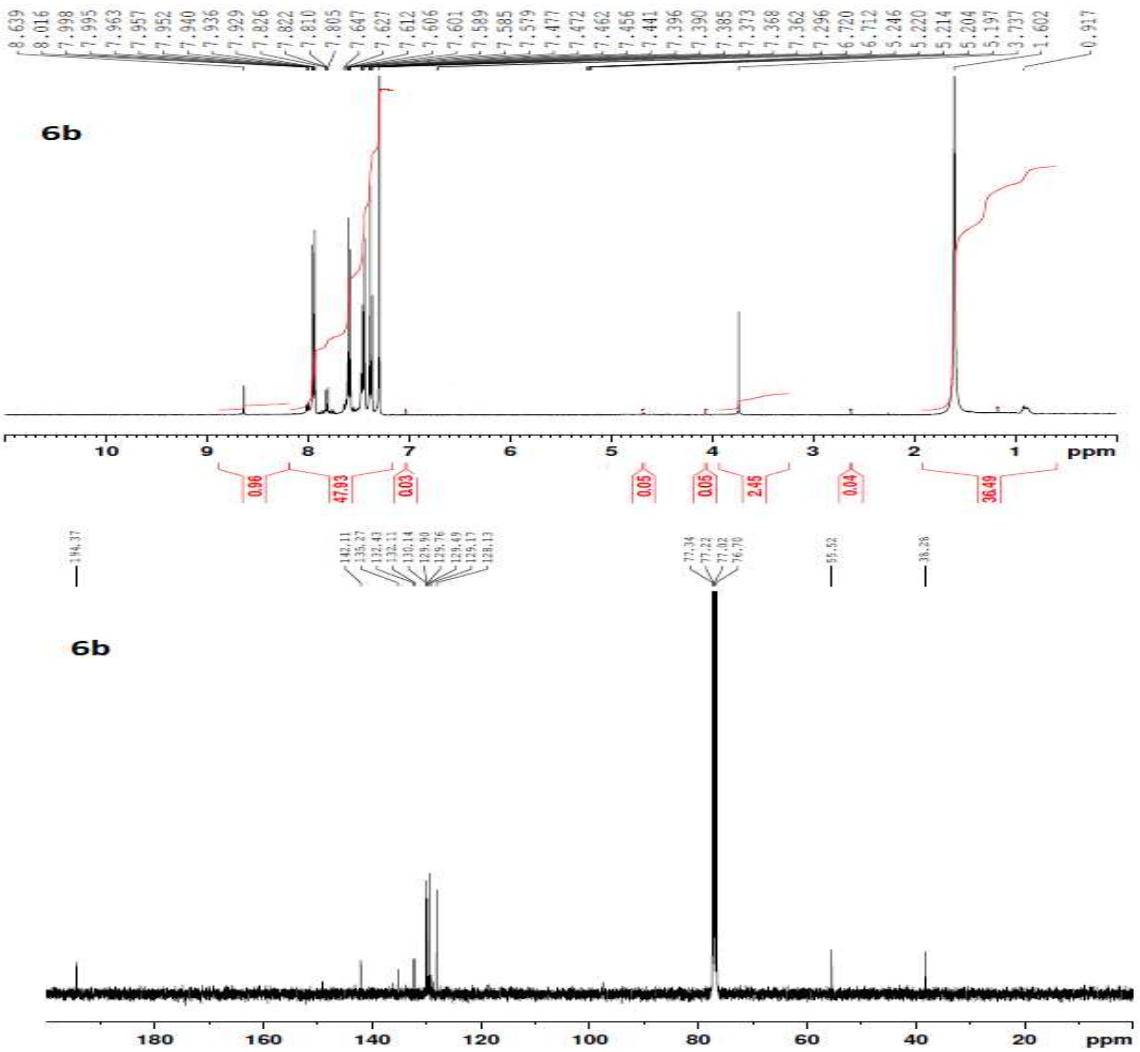

Fig. 2. NMR spectra of 4-((4-Chloro-benzylidene)-amino)-5-trifluoromethyl-3-((4-methyl-phenyl)-2-oxoethyl)thio-4H-[1,2,4]triazole (6b, CATM) derivative

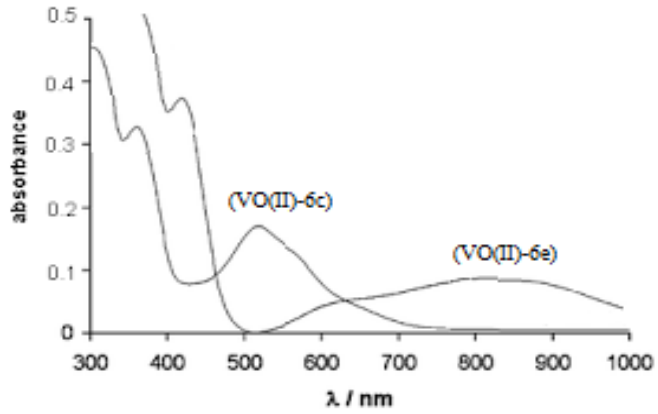

Fig. 4. UV-Vis spectra for two selected complexes

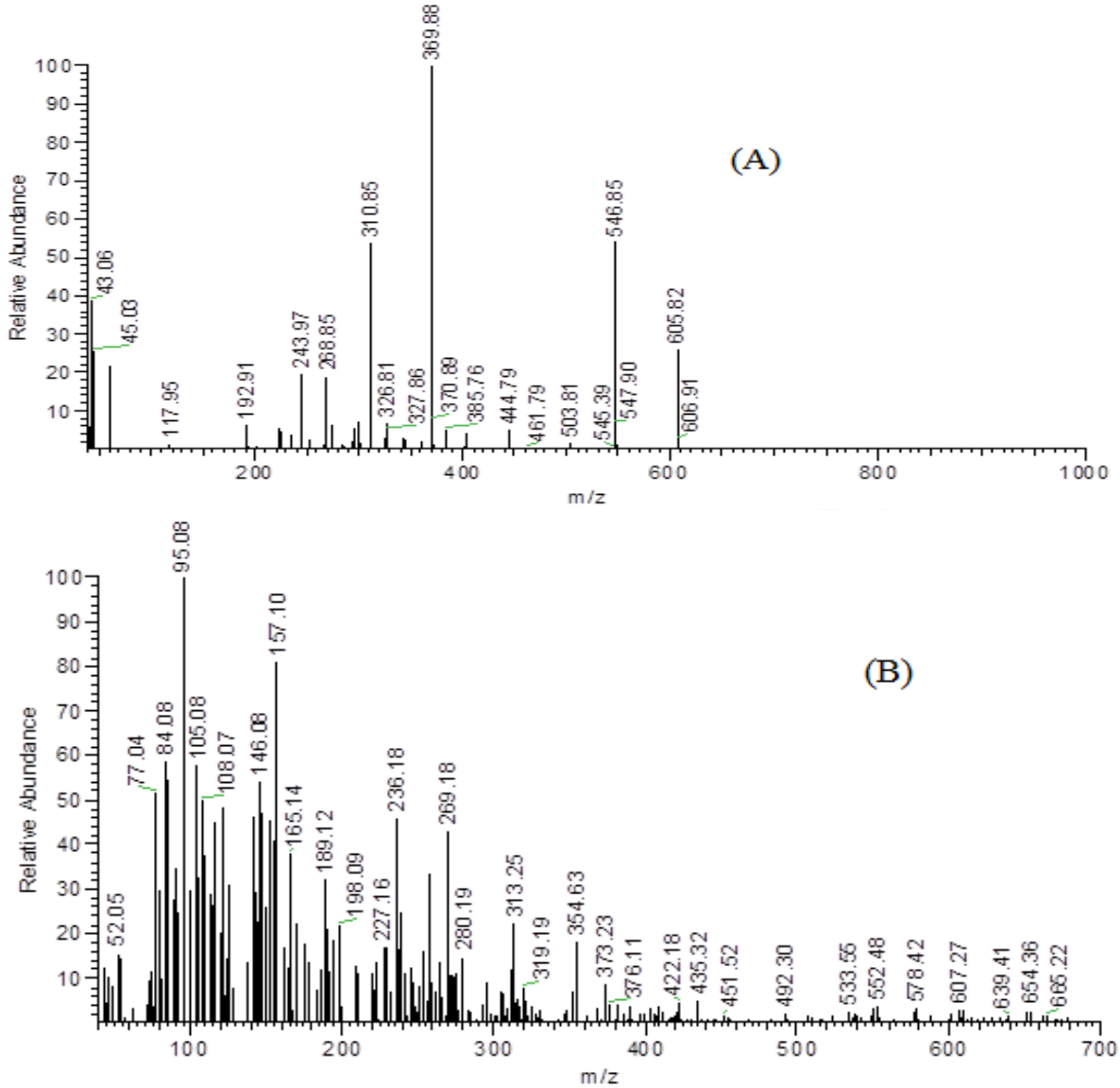

Fig. 5. Mass spectra of [VO (CATP)(H_2O)](SO_4)(H_2O)$_2$ (A)and [VO SO_4(CATB)] (B) complexes

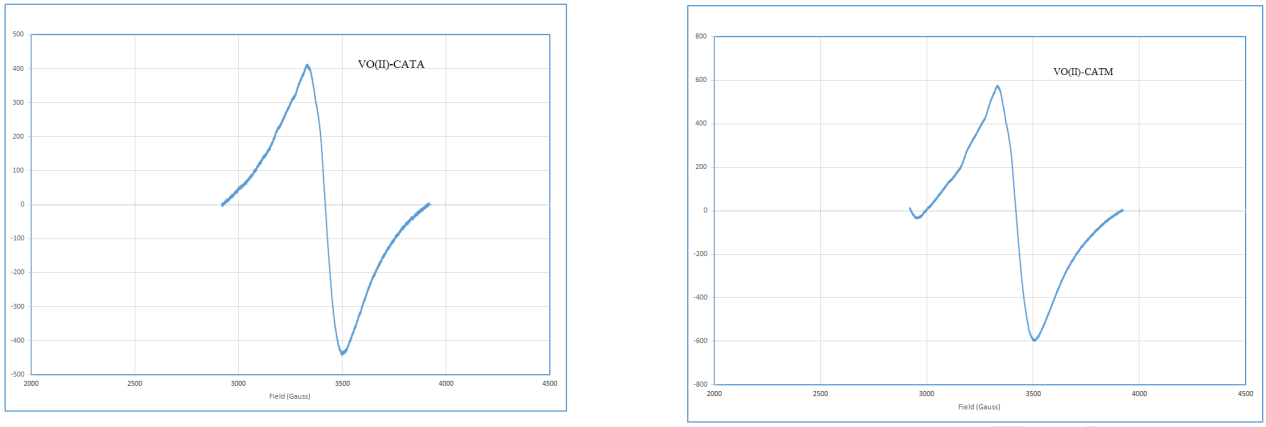

Fig. 6. EPR spectra of two complexes

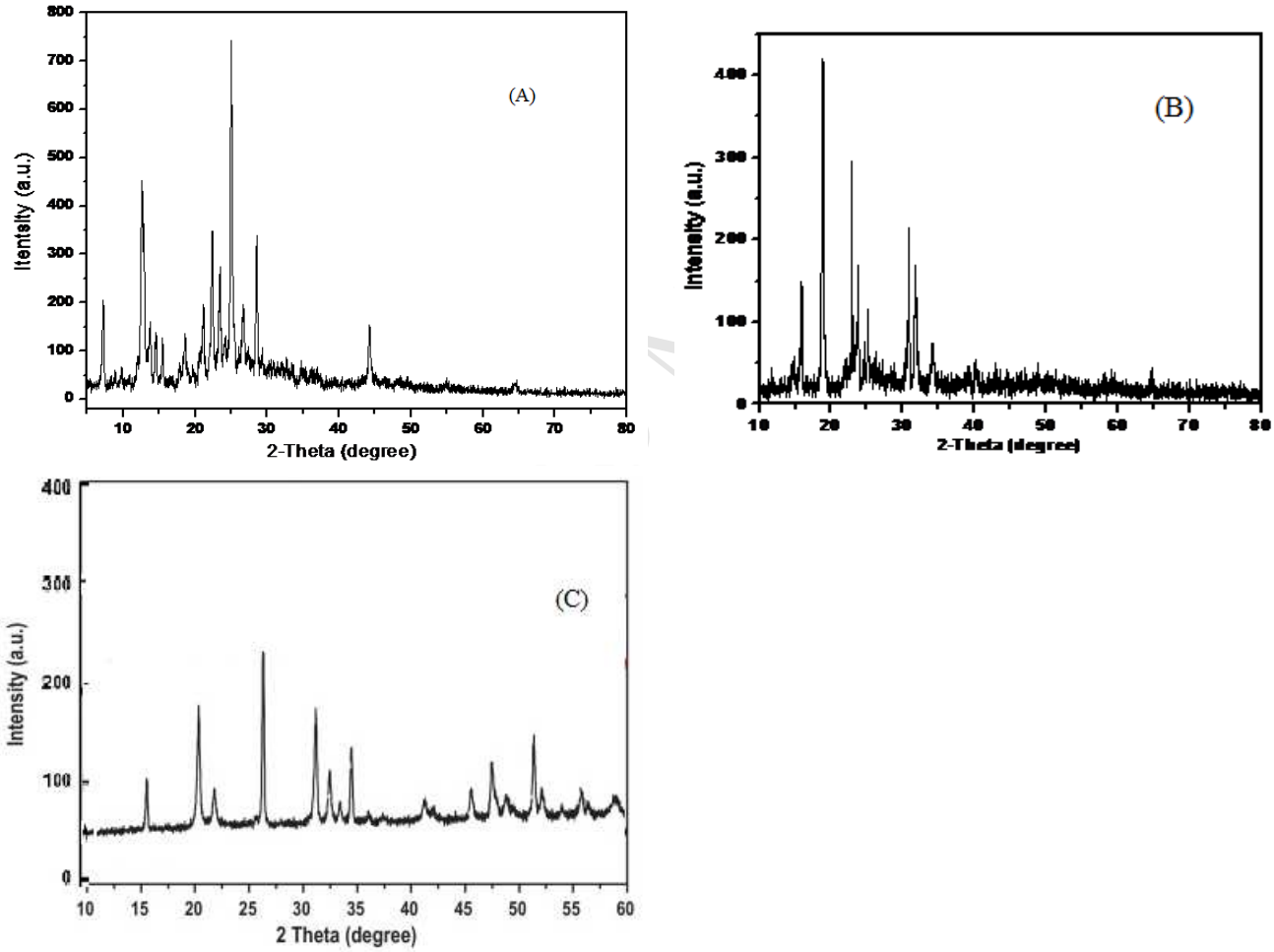

Fig. 7. XRD of $[VO\,SO_4(CATM)]2H_2O$ (A), $[VO\,SO_4(CATB)]$(B) complexes and V_2O_5 (C) oxide

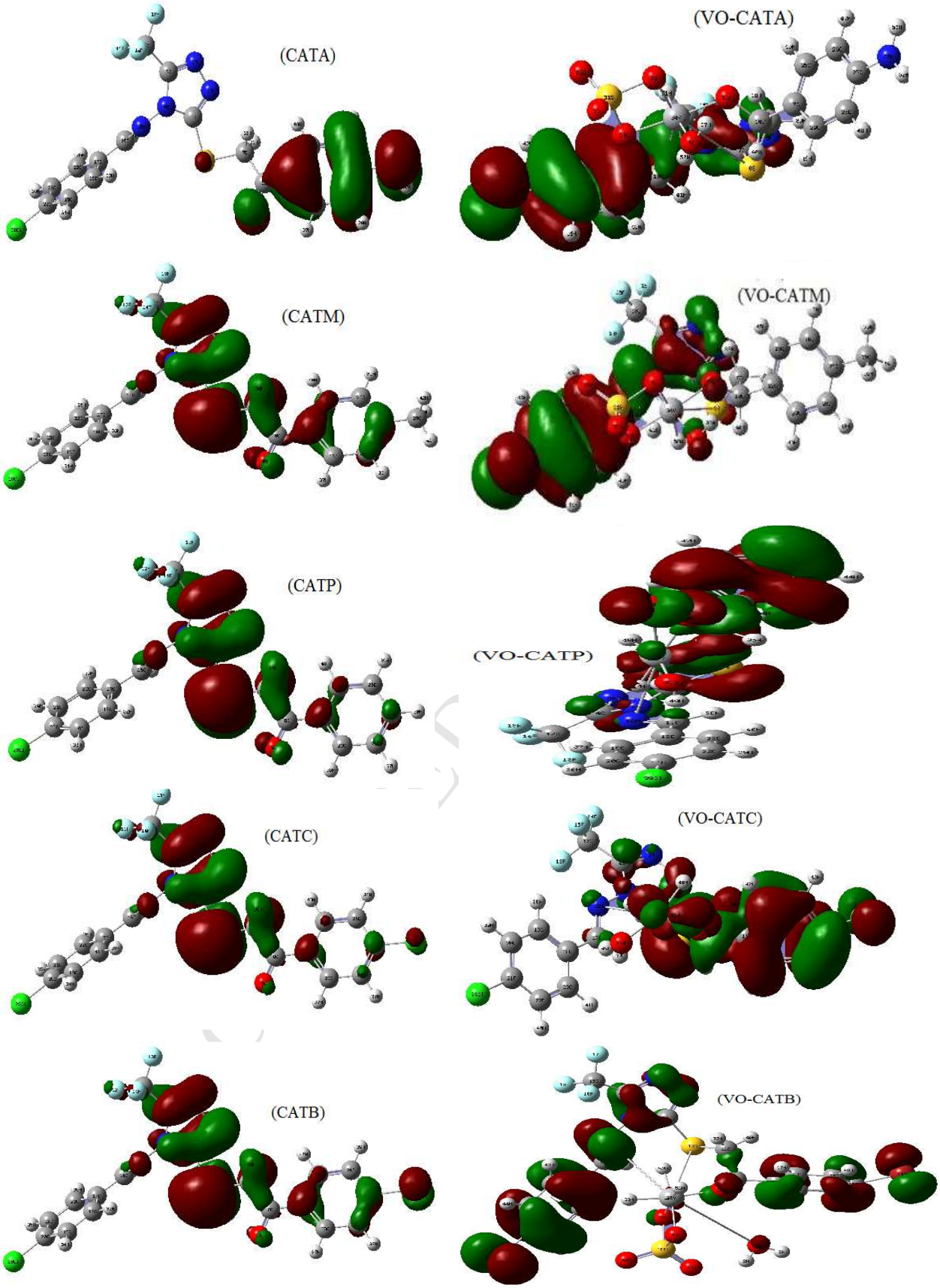

Fig. 8. Images of HOMO levels of traizole derivatives and their VO(II) complexes

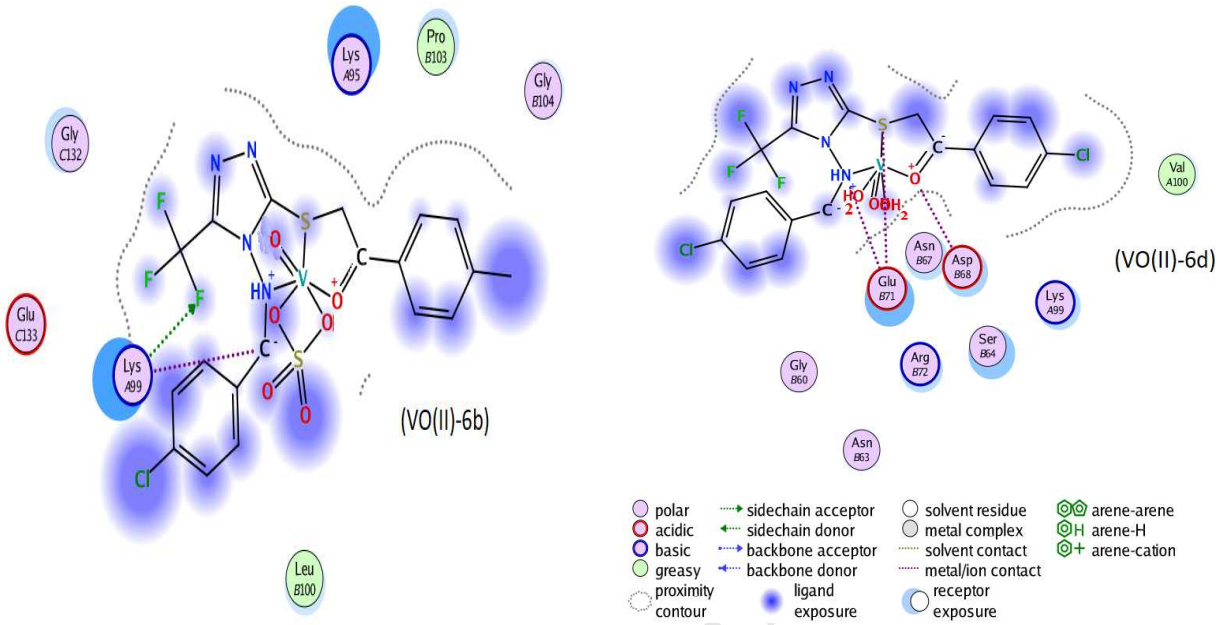

Fig. 9. Docking validation for two complexes interactions against DNA- protein receptor (2hio)

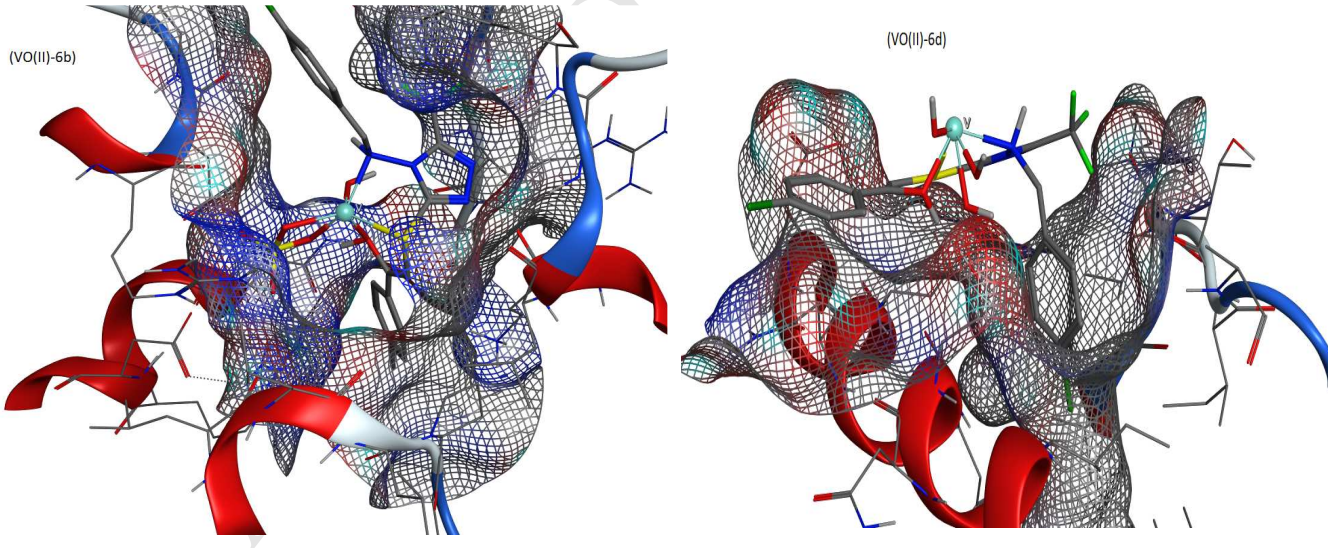

Fig. 10. Superposition of selected inhibitors in binding sites against DNA- protein receptor (2hio)

1- Synthesis for new VO(II) complexes from five thaizole derivatives
2- Characterization for all synthesis by all possible tools, among them was mass spectra for two selected complexes
3- Theoretical conformational tools were implemented in this study to strengthen the discussion part
4- Docking displayed lower biological activity for investigated complexes
5- The catalytic activity was implemented to synthesize biodiesel from waste olis